MEDWIN PUBLISHERS
Committed to Create Value for Researchers

Physical Science & Biophysics Journal
ISSN: 2641-9165

Construction of Rotation Channels for Pathogens Using the Repacking Method of Elements from Metamaterial Penetrated By Ultraviolet C Radiation

Starodub E, Munteanu I, Bazgan S, Podoleanu D, Costisen I and Enaki NA*

Quantum Optics and Kinetic Processes Laboratory, Institute of Applied Physics, Republic of Moldova

***Corresponding author:** Nicolae A Enaki, Quantum Optics and Kinetic Processes Laboratory, Institute of Applied Physics, Ministry of Education, Culture and Research, Republic of Moldova, Academiei str. 5, Chisinau, Moldova, Email: enache_nicolae@yahoo.com

Review Article

Volume 7 Issue 2

Received Date: October 17, 2023

Published Date: October 30, 2023

DOI: 10.23880/psbj-16000256

Abstract

Our proposal involves a novel approach to fluid decontamination, targeting substances like aerosols, infected water, blood, and plasma. We aim to achieve this by employing a combination of repacking methods involving both large and small elements within a metamaterial. This strategy is formulated to generate rotational pathways that enhance the movement of pathogens in regions with elevated ultraviolet C radiation, specifically at a wavelength of around 260 nm. Through the utilization of two key mechanisms, repacking, and centrifugal manipulation, we plan to create a groundbreaking decontamination method. In this procedure, we optimize the contact area by repacking a foundational structure made up of transparent spheres with smaller ones. Concurrently, we design helical channels resembling those found in centrifuges to manipulate pathogens such as viruses, bacteria, fungi, and aerosols within regions exposed to heightened ultraviolet C radiation. Our research reveals that as we reduce the size of the repacked components within the transparent metamaterial, the centrifugal force acting upon them intensifies. This effect directs pathogens and aerosols toward the evanescent region of the metamaterial, where the concentration of ultraviolet C radiation is elevated.

Keywords: Contact Surface in Decontamination; UV-C Radiation; Rotation Channels; Decontamination; Contaminated Fluid

Introduction

Recently the improving possibilities of the enhancement of the effectiveness of decontaminating various fluids such as aerosols, water, blood, and blood plasma through the application of ultraviolet C electromagnetic radiation within the wavelength range of 200-280 nm, has been a focus of the numerous recent studies described in References [1-6]. As a rule, contaminated fluids contain numerous particles, such as emulsions in liquids and aerosols in gases. To ensure comprehensive decontamination, it is essential to introduce a UV-C radiation dimer into the fluid, allowing it to penetrate the entire flow volume within the decontamination equipment. Our proposal involves combining both large and small elements of metamaterial within a unified matrix using a repacking procedure. This matrix of voids serves as a conduit for guiding the UV-C radiation deeper into the fluid. Ultimately, the smaller elements assist in redistributing

the guided waves throughout the localized volume of the decontamination fluid. This research aims to investigate how geometric repackaging techniques, applied to composite metamaterials composed of fibers and quartz balls, impact the fluid decontamination process. The objective is to enhance the decontamination rate by examining how various repackaging methods influence the interaction between the metamaterials and the treated fluids.

The advancement in decontamination equipment for liquids and gases has led to significant improvements in the interaction between pathogens and UV-C radiation. This progress is primarily attributed to the implementation of a more compact design and the repackaging of both larger and smaller elements within optical materials. This report suggests a strategy of densely packing metamaterial elements of varying sizes to achieve two key objectives. Firstly, it aims to enable deeper penetration of UV-C radiation into translucent liquids, thereby enhancing the effectiveness of the decontamination process. Secondly, it seeks to enhance the contact surface between the contaminated liquid and the UV-C-absorbing area of each element within the composite material. The propagation of UV-C radiation through the whispered gallery modes (see References [7-9]) of large spherical or fibrous elements enables the radiation to penetrate deep into the contaminated liquid. In the dynamic regime of decontamination, the above procedure of repacking, put the fluid to flow under the screw channels between the small elements of metamaterial so that that on the particles and suspense from the fluid acts the centrifugal forces which canalized the pathogens in the evanescent zone of hollows metamaterial where the rate of decontamination depends on the ultraviolet intensity of each zone. Additionally, the interaction between small elements and large elements facilitates the scattering of UV-C radiation throughout the active decontamination zone. Overall, this approach allows for more efficient utilization of UV-C radiation, enabling it to reach greater distances within the contaminated liquid while maximizing the interaction between the radiation and the pathogens present in the fluid. This study centers around the utilization of different geometric methods to package elements within a metamaterial, specifically designed to facilitate the accelerated movement of pathogens through the material via screw channels.

Close Packing Possibilities of Elements of Metamaterial

Below we give a short communication of packing structures of hole metamaterial consisting of small spherical elements with different structures and give the proprieties of propagation gallery ultraviolet C modes through the surface of these materials. One of the main points of this communication consists of the double centrifugal acceleration of fluids through holes created between the elements of metamaterials during the repacking. Let us begin with the holey metamaterial constructed from spheres with the same dimensions. If cubic packing is employed, a notable observation is the presence of numerous parallel and perpendicular channels that facilitate the unimpeded flow of liquid without significant alterations in its direction. However, when the second row is packed differed. There are two simple regular lattices that achieve this highest average density. They are called face-centered cubically, specifically in a square pyramidal arrangement; a significant departure from quasi-rectilinear fluid movement between the spherical particles is evident (see Figure 1). Transitioning from one layer to another necessitates the liquid circumventing the spherical particles via a four-step process, involving repacking.

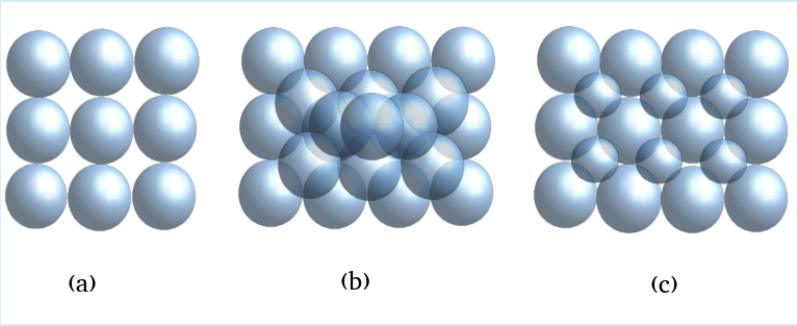

Figure 1: There are some types of so-called face-centered cubic (FCC) packing.

We are interested in the good optical contact between the balls so that the first layer of square packing (a) can be continued with the same balls into the second layer (b). But this form of packing doesn't give good optical contact with neighboring spheres, so the second layer is filled up with smaller spheres that have good contacts with 8 spheres between the layers, as this is represented in Figure 2A.

Consequently, if the liquid were to maintain the same velocity through both structural configurations, the liquid particles within the second arrangement would experience centrifugal acceleration while bypassing the obstructing spherical particles, thereby hindering the rectilinear laminar flow of the liquid. An additional consideration is that the spherical particles possess transparency in the ultraviolet C spectrum. This property is significant as the particles in the liquid, particularly those with higher densities such as pathogens and aerosols will adhere to the surface of these spheres due to the centrifugal acceleration obtained during their bypassing [10]. As ultraviolet C radiation effectively permeates through the spherical particles, the pathogens are compelled into the region where the radiation can exert its decontaminating effects. Consequently, through this manipulation of higher-density particles within the liquid, the efficacy of the decontamination process can be substantially enhanced.

Upon conducting a thorough calculation within a tightly arranged cubic lattice, one could initially surmise that the spheres precisely align with four spheres from the preceding layer and an additional four spheres from the subsequent layer, thereby accommodating the presence of precisely one sphere. However, a contrasting scenario unfolds when considering the configuration involving four spheres positioned below and four spheres positioned above. In this instance, it is possible to identify a sphere possessing a smaller radius than its counterparts, $R_x = R\left(\sqrt{3}-1\right) < R$ (see Figure 2A). Evidently, the centrifugal force exhibits a direct relationship with the mass of the particle (or pathogen) multiplied by the square of the average velocity of the fluid, while concurrently displaying an inverse correlation with the radius of the spherical particles. Consequently, the implementation of the repacking mechanisms involving smaller spherical particles precipitates a magnification of this centrifugal force, $F = \mathrm{mv}^2 / R_x$.

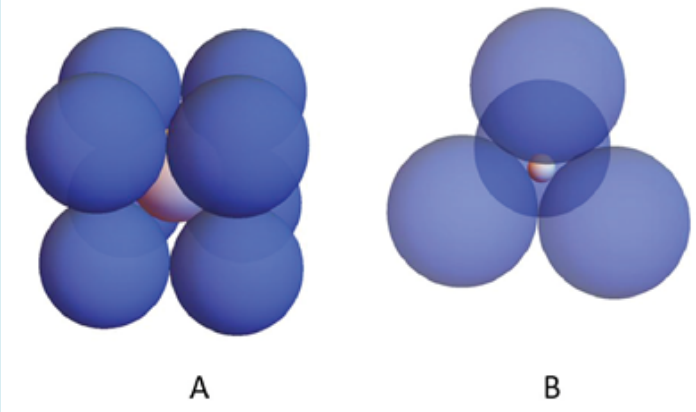

Figure 2A: The repacking of cubic lettuce with smaller spheres with radius $R_x = R\left(\sqrt{3-1}\right)$ less than the radius of big spheres of the metamaterial, R. B. The repacking tetrahedral cell with smaller sphere with radius $r = \left(\sqrt{3/2-1}\right)R$.

The arrangement of the balls can be altered through a repacking process, resulting in a hexagonal configuration, illustrated in Figure 1C. In this revised arrangement, the second layer of balls is positioned between three neighboring balls, forming an equilateral triangle. The fundamental building block, or unit cell, of this hexagonal lattice arrangement, can be described by the elementary cell consisting of a tetrahedral pyramid with four faces, all of which consist of equilateral triangles. Given that the fluid traversing through the interstices of the tetrahedral pyramids necessitates encountering augmented centrifugal acceleration, it is plausible to repack these structures by introducing smaller spherical particles at the central region of the tetrahedron. To ensure an appropriate configuration, the radius of the smaller spheres should conform to the relationship expressed as $r = \left(\sqrt{3/2-1}\right)R,$ here R represents the radius of the larger spheres in the principal matrix (see Figure 2B).

A noteworthy observation pertains to the substantial disparity in radii between smaller and larger spheres. In this context, the smaller spheres exhibit a marked reduction in size, approximately 0.22 times smaller compared to their larger counterparts. This substantial size differential has the potential to yield a significantly heightened acceleration experienced by pathogens present within the system.

In the context of crystalline packing, it is imperative to underscore the influence of Ultraviolet C radiation. This radiation permeates the entire crystalline arrangement, thereby expanding the zone of decontamination. The extent of this decontamination zone is directly correlated to the product of UV-C radiation's penetration depth within the surrounding fluid and the surface area occupied by the spheres comprising the crystal lattice. Notably, the penetration depth, denoted by D, is contingent upon both the refractive index of the spheres and that of the surrounding

fluid.

Building upon this concept, we propose a strategy to enhance the effectiveness of decontamination by amalgamating thick and thin elements within composite metamaterials, comprised of either quartz spheres or optical fibers. The primary aim is to attain the desired decontamination results while minimizing the repacking of the material and concurrently augmenting centrifugal force as the radius of the "optical obstacle" diminishes. In pursuit of this objective, we conducted a comprehensive reassessment of all packing structures generated through the ball/fiber packing method. Our specific focus lies in the unoccupied space that persists amidst the larger spheres. This space can be quantified in terms of sphere packing density within each metamaterial cell, with the cell density contingent upon the specific packing configuration adopted for the metamaterial Figure 3.

This approach takes into account the decontamination efficiency and the contact surface properties among the components of the metamaterial, such as photonic crystals or photonic crystal fibers, as elucidated in our experimental investigations [11-14], we propose to use the combination of elements of metamaterials like spheres/fibers in the close packing procedure, which form in principle the good material for the propagation of UV-C radiation and contaminated liquids/gases penetration in it. For this, we define the packing density, ρ, of a packing of spheres as the fraction of a volume filled with spheres and the free volume. Traditional in three dimensions, there are three periodic packing for identical spheres: cubic lattice, face-centered cubic lattice, and hexagonal lattice. Kepler hypothesized proposed in 1611, has been demonstrated by C. F. Gauss [15-19], according to which the highest average density has the order $\rho \sim \pi/(3\sqrt{2}) \sim 0.74$. We revised all packing structures formed by the ball packing method. We are interested in the remaining free space between the big balls, which may be expressed through the atomic packing density in each metamaterial cell, $V_f = V(1-\rho)$.

The free volume in the above example is so that in tetragonal packing, we have more free space than in hexagonal one. Following this example, we want to find the efficient decontamination volume which is proportional to the contact surface of the contaminated liquid with such packing balls. Taking into consideration that the penetration depth, k, on the free space between the balls is the proportional wavelength of radiation and inversely proportional to the difference between the refractive index of metamaterial, n_m and contaminated fluid $n_f, \kappa \sim \lambda/[2\pi\sqrt{n_m^2 - n_f^2}]$ (see for example Reference [9]), we can find this effective volume $V_u = \kappa S$, where S is the contact surface of metamaterial with contaminated fluid. Let us demonstrate that this volume is smaller than the free volume between the balls, V_f . According to the relation between the surface of the ball and its diameter, d, we find the dependence between the total surface number of balls and their diameter, $S = \pi d^2 N$. Representing the number of the balls in the l direction of the space $(l = x, y, z)$ with the volume, $V = L_x L_y L_z$, filled up by the number of spheres in each direction $N_i = L_i / d$, it is easy to find the total number of spheres in the box $N = N_x N_y N_z$. This number is proportional to the volume $N \sim V / d^3$. Now the decontamination efficient volume around the ensemble of packing balls is proportional to the penetration depth, $\kappa \sim \lambda$, and inverse proportional to the diameter of the balls, $V_u \sim V\lambda / d$. Only for the small diameter of the balls $d \sim \lambda$, it can achieve the free volume between the balls described by the free volume V_f.

According to the literature [15-20], we may estimate the occupied volume in following lattices: for cubic is $\pi/6. \approx 0.5236$, for tetrahedral lattice is, $(\pi\sqrt{3})/(1\,6) \approx 0.3401$; for hexagonal is $\pi/(3\sqrt{3}) \approx 0.6046$; random packing is 0.6400, for face- centered cubic close packing is 0.7405. To win in the contact surface, we fill up the free space between the elements of metamaterial with other small elements. We observe that the total surface of i -species of balls, $S_i = 4\pi V_{\text{fi}} / d_i$, where $V_{\text{fi}} = V(1-\rho)^{(i-1)}$ is the free volume remain free volume after introducing the spheres with the dimension d_{i-1}. Here the diameter d_i of i -type of spheres is smaller in comparison with earlier proposed equipment. We are focused on the applying of various geometry of packing elements of composite metamaterials like photon crystal to substantially increase the UVC decontamination contact surface with fluids and received an expected result for decontamination rate. We also propose the new more compact decontamination equipment for liquids and gases based on the idea of the construction of composite metamaterials from micro- to nano-levels using the optical contact between synthesized metamaterial elements with various structural dimensions using repacking technologies necked with the diameter of the i -1 sphere type by the relation $d_i = K^{-1} d_{i-1}$, here K^{-1} is ordered parameter less than unity. If we introduce a second types of spheres in the free space of cubic lattice, we obtain the following expression for the total surface, $S = S_1 + S_2$. Here $S_1 = \pi d_1^2 N$, and $S_2 = \pi N(\sqrt{3}-1)^2 d_1^2$ are the surface of the big and small spheres situate in the two lattices with the same number of nodes, N in optical contact. We not that the small spheres with diameter $d_2 = (\sqrt{3}-1) d_1$ are situated in the center of the cubes of the big one and don't have direct contact, where $K = 1/(\sqrt{3}-1)$. The total contact surface with contaminated fluid increases $S = \pi d_1^2 N(5 - 2\sqrt{3})$ with $0.5\,6 S_1$ relative, the metamaterial consisted of the packed spheres with the same diameter.

We can continue to introduce the small spheres into the cubic crystal. After the packing of the spheres in the center of the cube, we introduce the spheres in the face of each cube's surface. For this, we estimate the distance between the small spheres with diameter $d_3 = d_1 - d_2$ and distance between four big spheres $d_3^* = d_1\left(\sqrt{2}-1\right)$. We observe that the diameter $d_3 = d_1\left(2-\sqrt{3}\right) \sim 0.2\,8d_1$ is smaller than the diameter $d_3^* \sim 0.4d_1$. In this case, we can introduce the small sphere in the face of the cube with diameter $d_3 = d_1\left(2-\sqrt{3}\right)$, but we observe that each sphere has only two optical contacts with two centered spheres with diameter d_2 in adjacent cubes (See Figure 3A1). It is not difficult to observe that such spheres are unstable in this packing configuration and can relax in four points of the free volume contacting the big spheres in the face. In this case, the possibilities to obtain a stable periodic construction if we will introduce for the packing instead of the spheres, the rotation ellipsoids with big and small diameters $\left(d_3, d_3^*\right) = \left(d_1\left(\sqrt{2}-1\right), d_1\left(2-\sqrt{3}\right)\right)$. The total contact surface with fluids increases substantially to $S = S_1 + S_2 + S_3$, where for all elementary cell of the crystal we have three small spheres in the face of one cell, $S_3 = 3\pi \mathrm{N}\, \mathrm{d}_3^2 = 3\pi \mathrm{N}\, \mathrm{d}_1\left(7-4\sqrt{3}\right)$. As followers from above discussion, these two points close packing for spheres is not so stable because a small fluctuation of green sphere coupled with four big one destroys the optical contact between two of them. But these spheres passed in the hollow space between two big and one middle spheres with diameter d_2. In these hollows we can introduce the four spheres with diameter $d_3 \sim d_{3x} < d_3^*$ in each face of the cube to obtain the stable packing as this is represented in Figure 3A2. In this case in the elementary cell, we have 12 such spheres and the decreasing of diameter of each sphere does not go to decrease of the total surface at each level of repacking. A similar conclusion may be done for tetrahedral packing of spheres represented in Figures 3B1 and B2.

As the repacking procedure of hollows between the big spheres with small one passes into unstable system and to obtain the stabile, we need to use the smaller spheres in face as this is represented in Figures 3A2 and B2, it is convenient to fill up the hole space between the spheres with k times smaller spheres than initial packed matrix.

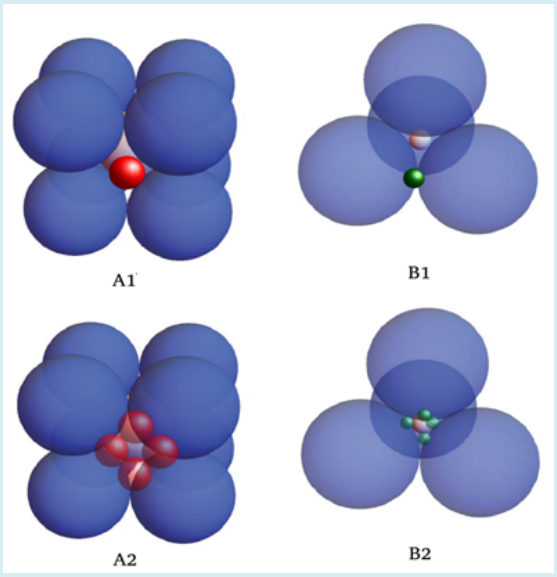

Figure 3: The illustration, A, represents the face repacking of cubic lettuce with smaller spheres with radius $R_x = R\left(\sqrt{3}-1\right)$ less than the radius, R, of big spheres of the metamaterial, and the image, B, represents the repacking tetrahedral cell with smaller sphere with radius $r = \left(\sqrt{3/2}-1\right)R$.

Similar conclusions may be reached and for the packing procedure of the fibers with different diameters and the same length see Reference [5]. In this situation, the square packing of fiber with diameter d_1 permits the filing up the free space between them by fibers with the smaller diameter, $d_2 = d_1\left(\sqrt{2}-1\right)$, in the close packing procedure represented in Figure 4 and 5C. The total surface of the fibers increases and becomes the sum of the thick and thin fibers $S_t = S_1 + S_2$.

Here the total surface of the first or second fiber type is equal to the product of the perimeter of the circle multiply by their number and length, $S_i = \pi d_i \mathrm{L}\, \mathrm{N}_i$. For the thick fiber, we can find the relation between their number, N_1 and diameters of the fibers, d_1 and d_2, the dimension of the packing box, D,

where these fibers are packed. Indeed, considering that these fibers filed up the square with length D, we can easily approximate the side of the square by $D = N_x d_1$. As the square has the same number of fibers along the x and y sides, we can observe that $N_x = \sqrt{N_1}$, where $N_1 = N_x N_y$. In other words, the total surface of the packing fibers with the same diameter is $S_1 = \pi \mathrm{DL}\sqrt{N_i}$. The similar conclusion may be obtained and by cylinder $S_i \sim \mathrm{DL}\sqrt{N_1}$ which squeezes the unused space in the decontamination procedure of the fluids References [11,12,14]. For thin fibers the estimations are similar with thick one $S_2 = \pi \mathrm{DL}\sqrt{N_2}\left(\sqrt{2}-1\right) = S_1\left(\sqrt{2}-1\right)$. In the procedure of close packing of fibers, we obtain the win in the total decontamination surface with a value of about 0.4 4.

We note that the crystalline packaging with smaller fibers/spheres has achieved an unstable construction. In this situation, to improve the decontamination rate, it is better to take the fibers/spheres with a diameter of $5-1\ 0$ smaller than the distance between the thick fibers (big spheres) and study the total contact surface with the contaminated fluid. If we consecutively pack spheres, we get the next improved total contact area, S_{tn}, with the contaminated fluid flowing by the metamaterial obtained

$$S_{\mathrm{tn}} =_{-} S_1 + S_2 + \ldots + S_n. \qquad (1)$$

Taking into account the analytical expression for each type of the packing fibers/spheres, $S_i = t\pi V(1-\rho)^{i-1}/d_i$, we obtain the new relation for the total contact surface, $S_i = t\pi V(1-\rho)^{i-1}/d_i$, where $t = 4$ for spheres and $t = 1$ for fibers. The total surface of the composite assembly formed from n - types of fibers/balls becomes equal to the expression

$$S_{\mathrm{tn}} = \pi \mathrm{t\ V}/d_1 + 4\pi \mathrm{t\ V}(1-\rho)/d_2 + \pi \mathrm{t\ V}(1-\rho)^2/d_3 + \ldots + \pi \mathrm{t\ V}(1-\rho)^{n-1}/d_n. \qquad (2)$$

Where $q = (1-\rho)K$. In the example above $K = 1\ 0$. Maybe the situation in which the last term of the expression (equation 2) gives the main contribution to the total surface of metamaterial. This is realized when the geometric progression ration is larger than unity, $q > 1$. In this situation, the main contribution in total surface (2) gives the surface with the smallest diameter. In this situation, $(1-\rho) > K1$ the total area of composite metamaterial drastically increases with decreasing of diameter, $d_n = 1\ 0^{-(n-1)} d_1$, of the smallest packing fraction. But analytically expression takes into consideration and other situations in which for $K > 1$ and $(1-\rho) < 1$ is realized unity value of the geometrical progression ratio, $q = (1-\rho)K \sim 1$. In this situation, all species of quartz balls with diameter, $d_i = d_{i-1}/K$, give a substantial contribution in the composite metamaterial. The rotation channels between the fibers can be made by twisting the set of fibers and gluing it at high temperatures if necessary for fragile fibers, as shown in Figure 5C.

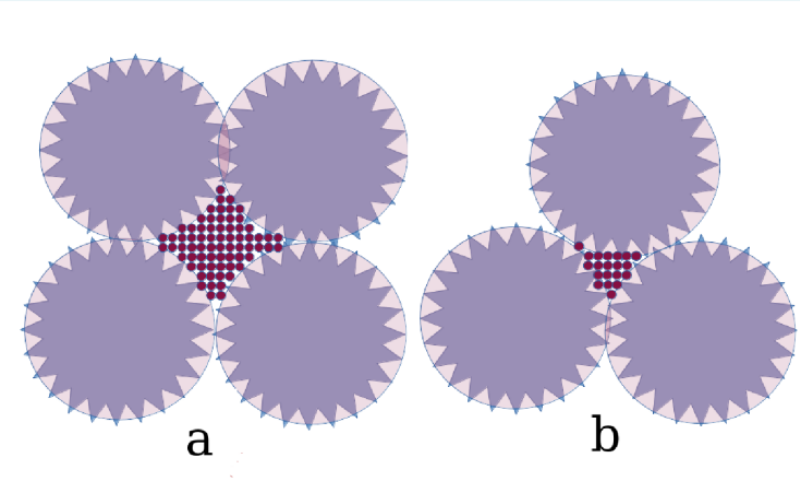

Figure 4A: The substitution of impenetrable space between the thick fibers with diameter d_1 filled up by thin fibers/spheres with diameter d_1/K in square packing of the two types of elements. B. The filled up of impenetrable space between the thick fibers (big spheres) by thin fibers (small spheres) in the hexagonal repacking with diameter $d_1 = d_1/K$. The procedure of constraint of the impenetrable by radiation space can be continued till the packing of the smallest spheres with diameter $d_n = d/K^{n-1}$.

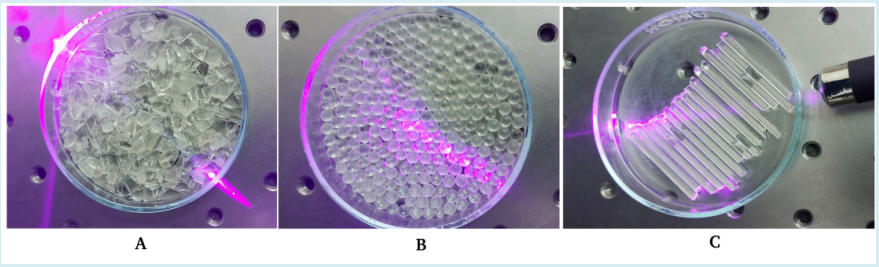

Figure 5: A. Possible realization of the screw channel repackaged with the metamaterials formed by the dropped quartz with different sizes from $1\ 0^{-5}$ and $1-2$n m B. Realization of the close random packing of the small and big spheres. Figure C represents the optical fibers repacked in the decontamination of the core of the equipment so that the free space between them achieved minimal value. Each of these packaging models of the metamaterial employed in the decontamination process underwent exposure to blue laser irradiation.

Experimental Results and Discussions

We substituted these contaminated fluids with pathogens with yeast solution, which has larger resistance to UV-C radiation in comparison with many viruses or bacteria. According to the existing experimental data [21-24]. The resistance of fungi to prokaryotic bacteria and viruses is quite high. The various dimension of yeast fungus colonies before going through the decontamination system tested in 8 probes represented in Figure 6 was established on the number of probes more than "20". These yeast solution probes are represented in Figure 6 in which we observed the aleatory dependence of colony dimension in each probe. With increasing the dimension, the number of colonies per same decreases.

Our yeast solution belongs to Saccharomyces cerevisiae species with the proprieties to form the colonies, formed from unicellular organisms and having the ability to be arranged in strings of connected budding the yeast cells known as pseudohyphae or false hyphae [25-31]. Life within these populations is a prevalent form of microbial existence in natural settings that provides the cells with capabilities to effectively defend against environmental attacks as well as efficiently adapt and survive long periods of starvation and other stresses.

As a eukaryotic cellular construction, the yeast colonies oppose more large resistance to UV-C radiation in comparison with pathogen prokaryotic cellular colonies. Yeast sizes achieved the dimension $1-3\ 0\mu m$ in diameter and present an interest to study the evolution of the number of yeast colonies and their number before and after the decontamination procedure. For this, we propose to use the normal distribution of yeas colony numbers, n, and their diameters d.

$$W(n,d)=\frac{1}{\sqrt{2\pi}\,\sigma_n}\exp\left[-\frac{(n-n_0)^2}{2\sigma_n^2}\right]\times\frac{1}{\sqrt{2\pi\sigma_{d_n}^2}}\exp\left[-\frac{(d_n-d_{n_0})^2}{2\sigma_{d_n}^2}\right]. \quad (3)$$

Here $\sigma_{d_n}^2$ is the size variance, and σ_n is the numerical variance of yeast colonies for the same diameters d_n. For experimental results, we estimate the average prepared for decontamination of yeast solution. Before deactivation, we have $n_0=9;\ \sigma_n=2;\ d_{0n}/d_{\text{sp}}=0.0\,5/n_0$ and $\sigma_{d_n}=0,1/d_{\text{sp}}$ Here d_{sp} is the visualized diameter of the microscope image represented in Figure 6.

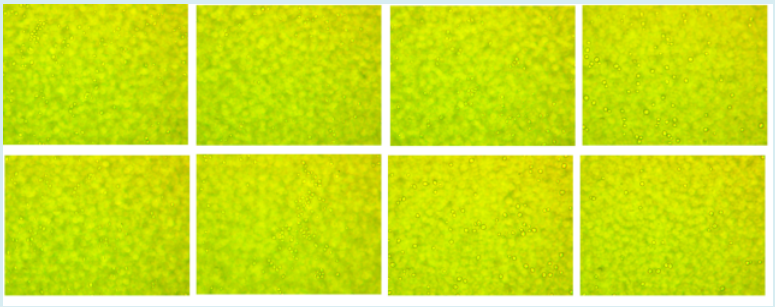

Figure 6: The various dimensions of yeast fungus colonies before going through the decontamination system tested in 8 probes. Mediation over the dimension and number of colonies was established on the number of probes more than 20. The 8 probes are represented in this figure. It is observed the dependence of colony dimension as the function on its number on the probe. With increasing the dimension, the number of colonies per same decreases.

Based on experimental observations, a significant portion of the liquid flow undergoes effective decontamination within duration of $t = 5\text{min}$. In Figure 5, we have introduced three different types of metamaterials designed for use within the decontamination core of the equipment, as depicted in the same figure. Upon careful examination in Figure 9, it becomes evident that the dimensions of these metamaterial elements have become smaller compared to their initial sizes, with a substantial proportion (approximately 70-80%) having been damaged. To underscore the importance of filling the space between the metamaterial elements, we propose another experiment. In this scenario, the large gaps between the quartz granules are filled with smaller granules, effectively reducing the unoccupied space that radiation cannot penetrate. This reduction in space between the metamaterial elements demonstrates a corresponding increase in the rate of decontamination, aligning with the theoretical predictions articulated in the preceding section. In the experimental setup illustrated in Figure 8B, a mixture of granulated quartz material with a wide range of granule dimensions (from $0.0\,1\,\text{cm}$ to 0.5c m) shows a significant improvement in decontamination efficiency when compared to the fiber system depicted in Figure 9C. This effect can be straightforwardly explained by the fact that the granule sizes facilitate the focused direction of radiation towards the center of the tube, which has a diameter of approximately 3.0 cm.

According to our theoretical discussion in Section 2, we may put three experiments with such metamaterials represented in Figures 7, 8 and 9. Two experiments contain the system of quartz balls with the dimensions " $d_1 \sim 1-2\text{m m}$ and fibers with diameter about $d = 1\text{m m}$. Another experiment contains crushed granulated quartz material represented in Figure 8 B. Here we have compared the contact surface of the quartz spheres and fiber optics system. The granulated quartz metamaterial with various dimension is proposed for an experiment in which in our opinion is realized the situation in which between the big elements are introduced the smaller elements of the composite metamaterial so that the total surface can be approximated by the sum of the surfaces of elements with the same optical characteristics $S_t = S_1 + S_2 + S_3 + \ldots + S_n$. The quality of decontamination depends on the method of granulating of the quartz balk during crushing. This effect was established during the measurements. All three types of metamaterials were introduced in the decontamination core, which consists of a quartz tube with a length of 100 cm and a thickness of about 3.0cm.

For the identification of the influence of packing geometry on the decontamination rate, it is proposed three experiments. After the 40 min of experimental treatment of yeast solution situation represented in Figure 4, the core of the decontamination equipment represented in Figure 10.

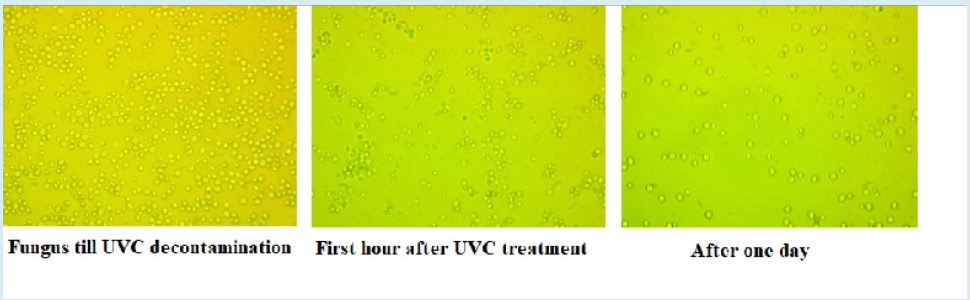

Figure 7: Decontamination with repacking spheres. The left figure represents the various dimensions of yeast fungus colonies before going through the decontamination equipment consisting of the core tube with a diameter of about 3.0 cm and length 1.0 m filled up with quart bubbles represented in Figure 6. The central figure represents the yeast fluid visualized on the optical microscope after its passing through the decontamination equipment during the5 min. As it is observed the optical microscope practically doesn't detect the yeast fungus. The right figure represents the increase of fungus colonies in the same "decontaminated" fluid after one day (24 hours). It is observed that the slight increase of the yeast colonies for one day.

The two types of quartz bubbles were packed in the core of the equipment represented in Figure 9. After 5 min of decontamination time interval the big number of yeast colonies were inactivated with fibers repacking see (Figure 9). In order to compare this metamaterial with quartz granules, we give the remaining yeast small fungus to increase during the 24 hours. This method gives us the possibility to estimate the decontamination rate of three types of the material described in Figure 9.

Figure 8: Decontamination with granulated metamaterial. A similar three figures were obtained for the decontamination core filled up with granulated metamaterial with a large variety of granules. It is observed that after one day the mean value of the new restoration colonies of the yeast fungus is smaller than in bubbles packing. The mean value of the new restoration colonies of the yeast fungus is smaller than in bubbles packing.

The role of the small granules in optical contact with the large one scattered the standing waves in the non-penetrating free space between the large granules. The yeast solution flowing through such space can't be decontaminated with the metamaterial formed from fibers/spheres with relatively greater dimensions in comparison with the smallest dropped quartz granules. Thus, the volume of decontamination (and decontamination rate) substantially increases in this case. According to the estimated data, for the same amount of liquid and the same amount of fungus, the above-mentioned composite decontaminates with a much better rate at the same time of exposure of the liquid to UV radiation. From the experiments observed there is a noticeable substantial decrease in the radius of fungus colonies and its number. In composite granulated metamaterial, it is observed the higher decontamination rate under the same exposure time and the same concentration of fungus colonies used in the fiber system.

Figure 9: Decontamination with repacked fibers. The last two figures (central and right) represent the decontamination procedure with two types of packing fibers in the decontamination core. As it is observed after the 5 min of the UV-C radiation some colonies continue to remain in the fluid. This relates to the remaining large intervals between the fibers during the laminar flow of the yeast liquid.

We comment on the experiment with quarts fibers, which consists of a 3.0 diameter quartz tube filled up with 1mm diameter quartz fiber. The decontamination volume is smaller than the free volume between the fibers due to the big distances between the 1- and 2-mm fibers in comparison with the UV-C wavelength. It is formed by the surface of all fibers, together with the surface of the quartz tube, s, multiplied by the radiation penetration depth κ, $V_u = (A+s)D$. The estimation demonstrates that for the free volume between three fibers of length 100 cm, and a diameter of 0.1cm can easily calculate. It is equal to the difference between the area of the equilateral triangle (like in Figure 4) and the three-circle segments which are at the approximation -degree angle to the length of the fiber $V_f = L(\sqrt{3}-\pi/2)r^2 = 0.16r2L,\quad r-$ is the radius of fiber $r = d/2$. The efficiency of the decontamination rate of the volume situated between these fibers of a big cylinder may be calculated in two ways. The first method corresponds to the calculation of the effective volume between three fibers. This corresponds to the volume is equal to the length of the three arc portions multiplied by the radiation penetration depth, $\kappa \sim \lambda/2,$ in the liquid: $V_u = \pi r\kappa L.$ It is not difficult to observe that ratio, $E_f = V_u/V_f \sim \lambda/r,$ is quite small for wavelength $\lambda \sim 250\text{nm} - 280\text{nm}$ and describes the contact efficiency. The free volume, V_f is the difference between the total volume of the big cylinder $V = \pi R^2 L,$ where $R = 2.5\text{cm},$ $L = 100\text{cm},$ and the volume of packed fibers in it, $V_m = \pi \text{Nr}^2 L,$

we can find the free volume $V_f = V - V_m = \pi\left(R^2 - \mathrm{Nr}^2\right)L.$

According to the experimental results represented in Figure 9 the good decontamination was obtained with granulated metamaterial. Not so bad decontamination rate in comparison with quartz granules was obtained with two types of packing bubbles. In this experiment, we don't have exactly the situation proposed in the theoretical conception of close packing spheres. But of course, the granulated metamaterial represents more plotted metamaterial and the decontamination volume of evanescent zones around the elements is larger than in two types of bubble packing. The two types of fiber systems were radiated perpendicular to the fibers. The yeast solution flows laminar between the fibers so that a lot of fungus colonies remain in the non-penetration space by UVC radiation. This may be the explanation for not so well decontamination rate. Here we don't use the fibers with a diameter less than 5 – 10 times smaller than the thick fibers. This also is an argument on the not so good decontamination rate in comparison with bubbles and granulated material.

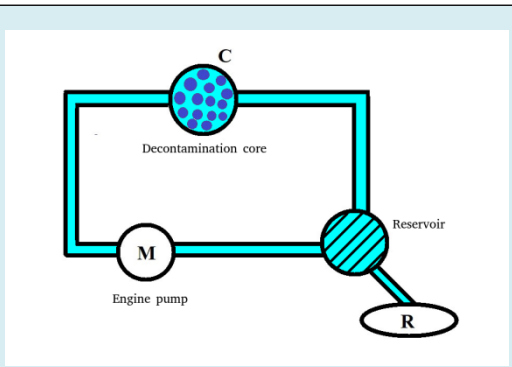

Figure 10: The contaminated fluid from reservoir is rotated by engine pump through decontamination core consisting from repacked metamaterials. The composition of hollow metamaterials was changed according to experimental results represented in Figures 7-9.

Conclusion

The suggested method for repacking transparent elements within an optical material aims to leverage unutilized space within the metamaterial to enhance decontamination efficiency by increasing the available surface area. This concept of repacking periodic structures with additional elements is a phenomenon observed in various complex crystal and glass structures, as documented in previous studies [32].

It also plays a specific role in multiple proteins, with complexes like tubulins assuming particular significance in cellular processes [33,34]. This paper introduces an innovative approach that capitalizes on the space between larger and smaller elements within a composite metamaterial to enhance the interaction between UVC radiation and the fluid. By repacking this space near the larger elements, we propose a new equipment design that can be employed for the decontamination of non-transparent fluids within the UVC wavelength range. The inclusion of multiple reflections of radiation within the metamaterial, combined with the utilization of an aluminum enclosure, provides us with the potential to elevate the decontamination efficiency of this equipment when applied in various conditions. This equipment has the versatility to be effective in different settings, including indoor environments with aerosols and non-transparent fluids contaminated with viruses and bacteria nanoparticles in water.

The integration of small and large components within a metamaterial introduces a novel avenue for creating optical connections between the larger elements and pathogens present in the fluid via the smaller granules within the composite structure. This concept involves harnessing the resonance penetration of radiation from one granule to another on a smaller scale. Such a mechanism could be harnessed for the transmission of UV radiation to the bio-molecular tissue within living cells. This becomes particularly relevant in scenarios where precise channeling of radiation into small regions for photo-transformation reactions is necessary, often presenting challenges in terms of comprehension and control.

Acknowledgment

This paper is supported by the projects: No. 20.80009.5007.01 and NATO EAP SFPP 984890.

References

1. Sabino CP, Ballc AR, Baptistad MS, Daief T, Hamblineg MR, et al. (2020) Light-based technologies for management of COVID-19 pandemic crisis. J Photochem Photobiol B 212: 111999.

2. Heling M, Hnes K, Petra V, Lingenfelder C (2020) Ultraviolet irradiation doses or coronavirus inactivation-reviewand analysis of coronavirus photoinactivation studies. GMS Hyg Infect Control 15: Doc08.

3. Kalyani VL, Prachi M, NupurM, Singhal N (2020) Study on Coronavirus (COVID-19) and how UVC Light helps to Destroy it and its Applications. Journal of Management Engineering and Information Technology (JMEIT) 7(3): 19-23.

4. Buonanno M, Welch D, Shuryak I, David JB (2020) Far-UVC light (222 nm) efficiently and safely inactivates

airborne human coronaviruses. Sci Rep 10(1): 10285.

5. Mack R (2020) Covid-19 and fiber optic cable assemblies. FOC News.

6. Baer TM, Baer CE (2020) Optics and the COVID-19 Pandemic. Optics & Photonics News.

7. Panitchob Y, Murugan GS, Zervas MN, Horak P, Berneschi S, et al. (2008) Whispering gallery mode spectra of channel waveguide coupled microspheres. Optics Express 16(15): 11067.

8. Yang Y, Wang Z, Zhang X, Zhang Q, Wang T (2023) Recent progress of in-fiber WGM microsphere resonator. Front Optoelectron 16(1): 10.

9. White IM, Zhu H, Suter JD, Hanumegowda NM, Oveys H, et al. (2007) Refractometric Sensors for Lab-on-a-ChipBased on Optical Ring Resonators. IEEE Sensor Journal 7(1).

10. Enaki NA, Starodub E, Paslari T, Turcan M, Bazgan S (2021) Increasing of Decontamination Rate of Infected Fluid by Rotation Channels under the Dispersion of Ultraviolet C Radiation by Composite Metamaterial. Phys Sci Biophys J 5(2): 188.

11. Enaki NA, Profir A, Ciobanu N, Bazgan S, Nistreanu A, et al. (2018) Optical metamaterials for decon-tamination of translucent liquids and gases. J Phys D 51: 385101.

12. Enaki NA, Bazgan S, Ciobanu N, Turcan M, Paslari T, et al. (2017) Improvement in ultraviolet based decontamination rate using meta-materials. Applied Surfaace Science 417: 40-47.

13. Enaki NA, Profir A, Bizgan S, Paslari T, Ristoscu C, et al. (2018) 13 Metamaterials for Antimicrobial Biofilm Applications: Photonic Crystals of Microspheresand Optical Fibers for Decontamination of Liquids and Gases. Handbook of Antimicrobial Coatings 13-27.

14. Enaki NA, Bazgan S, Nistreanu A, Tonu V, Turcan M, et al. (2018) Efficient microbial decontamination of translucent liquids and gases using optical metamaterials. In the book: Advanced Surface Engineering Research, IntechOpen 9: 169-197.

15. Gauss CF (1876) Review of the book by L. A. Seeber: Intersearches on the properties of positive ternary quadratic forms etc. Göttingsche Scholar Advertisements 2: 188-196.

16. Gardner M (2001) The Colossal Book of Mathematics: Classic Puzzles, Paradoxes, and Problems. W W Norton, New York, USA, pp: 128-136.

17. Jaeger HM, Nagel SR (1992) Physics of Granular States. Science 255(5051): 1523-1531.

18. Steinhaus H (1999) Mathematical Snapshots. 3rd(Edn.), Dover Publications, New York, USA, pp: 320.

19. Wells D (1991) The Penguin Dictionary of Curious and Interesting Geometry. Penguin, London, UK, pp: 237-238.

20. Hilbert D, Cohn-Vossen S (1952) Geometry and the Imagination. Chelsea, New York, USA, pp: 45-53.

21. Maier I (2010) CERTIFICATE: Inactivation of bacteria, viruses, and other pathogens by UV-C irradiation in the Leica cryostat product family. Ecoscope, Labor fur Mikrobiologie und Okotoxikologie, pp: 1-21.

22. Cadnum JL, Shaikh AA, Piedrahita CT,Annette LJ, Larkin EL, et al. (2018) RelativeResistance of the Emerging Fungal Pathogen Candida auris and OtherCandida Species to Killing by Ultraviolet Light. Infect Control Hosp Epidemiol 39(1): 94-96.

23. Dai T, Kharkwal GB, Zhao J, Denis TGSt, Wu Q, et al. (2011) Ultraviolet-C Light for Treatment of Candida albicans Burn Infection in Mice. Photochem Photobiol 87(2): 342-349.

24. Khan M, McDonald M, Mundada K, Willcox M (2022) Efficacy of Ultraviolet Radiations against Coronavirus, Bacteria, Fungi, Fungal Spores, and Biofilm. Hygiene 2(3): 120-131.

25. Yong E (2012) Yeast suggests speedy start for multicellular life. Nature.

26. Ratcliff WC, Denison RF, Borrello M, Travisano M (2012) Experimental evolution of multicellularity. Proc Natl Acad Sci U S A 109(5): 1595-1600.

27. Boraas ME, Seale DB, Boxhorn JE (1998) Phagotrophyby a flagellate selects for colonial prey: A possible origin of multicellularity. Evolutionary Ecology 12: 153-164.

28. Koschwanez JH, Foster KR, Murray AW (2011) Sucrose utilization in budding yeast as a model for the origin of undifferentiated multicellularity. PLoS Biol 9(8): e1001122.

29. Rosa C, Gbor P (2006) Biodiversity and Ecophysiology of Yeasts. The Yeast Handbook, Springer, pp: 580.

30. Walker K, Skelton H, Smith K (2002) Cutaneous lesions showing giant yeast forms of Blastomyces dermatitidis. J Cutan Pathol 29(10): 616-618.

31. Legras JL, Merdinoglu D, Cornuet JM, Karst F (2007) Bread, beer and wine: Saccharomyces cerevisiae diversity reflects human history. Mol Ecol 16(10): 2091-2102.

32. (2007) Complex Crystal and Glass Structures. In: Carter CB, Norton MG (Eds.), Ceramic Materials. Springer, Science+Business Media, LLC, New York, USA, pp: 100-119.

33. Binarová P, Tuszynski J (2019) Tubulin: Structure, Functions and Roles in Disease. Cells 8(10): 1294.

34. Barbier P, Zejneli O, Martinho M, Lasorsa A, Belle V, et al. (2019) Role of Tau as a Microtubule-Associated Protein: Structural and FunctionalAspects. Front Aging Neurosci 11: 204.